Txnip deletions and missense alleles prolong the survival of cones in a retinitis pigmentosa mouse model

Yunlu Xue[1,2], Yimin Zhou[2,3], Constance L. Cepko[1,4,*]

1. Departments of Genetics and Ophthalmology, Blavatnik Institute, Harvard Medical School, Boston, MA 02115
2. Lingang Laboratory, Shanghai, China, 200031
3. School of Life Science and Technology, ShanghaiTech University, Shanghai, China, 201210
4. Howard Hughes Medical Institute, Boston, MA 02115

*Correspondence: cepko@genetics.med.harvard.edu

Abstract

Retinitis pigmentosa (RP) is a prevalent inherited retinal degenerative disease worldwide, affecting 1 in 4,000 people. The disease is characterized by an initial loss of night vision followed by a loss of daylight and color vision. Many of the RP disease genes are expressed in the rod photoreceptors, the cell type that initiates dim light vision. Following loss of rods, the cone photoreceptors, which initiate daylight vision, also are affected and can die leading to total loss of vision. The reasons for loss of cone vision are not entirely clear, but appear to be due to loss of the rods. Previously we showed that overexpressing Txnip, an α-arrestin protein, in mouse models of RP using AAV gene therapy prolonged the survival of RP cones (Xue et al., 2021). At least part of the mechanism for cone survival was a switch in the fuel source, from glucose to lactate. In addition, the mitochondria of cones were both morphologically and functionally improved by delivery of Txnip. We have gone on to test several alleles of Txnip for the ability to prolong cone survival in *rd1*, a mouse model of RP. In addition, proteins that bind to Txnip and/or have homology to Txnip were tested. Five different deletion alleles of Txnip were expressed in cones or the retinal pigmented epithelium (RPE). Here we show that the C-terminal half of Txnip (149-397aa) is sufficient to remove GLUT1 from the RPE cell surface, and improved *rd1* cone survival when expressed specifically in the RPE. Overexpressing Arrdc4, an α-arrestin that shares 60% similar protein sequence to Txnip, reduced *rd1* cone survival. Reduction of the expression of HSP90AB1, a protein that interacts with Txnip and regulates metabolism, improved the survival of *rd1* cones alone and was additive for cone survival when combined with Txnip. However, full length Txnip with a single amino acid change, C247S, as we tested in our original study, remains the most highly efficacious form of the gene for cone rescue. The above observations suggest that only a subset of the hypothesized and known activities of Txnip play a role in promoting RP cone survival, and that the activities of Txnip in the RPE differ from those in cone photoreceptors.

Introduction

Retinitis pigmentosa (RP) is an inherited retinal degenerative disease that affects one in ~4,000 people worldwide (Hartong et al., 2006). The disease first manifests as poor night vision, likely due to the fact that many RP disease genes are expressed in rod photoreceptors, which initiate night vision. Cone photoreceptors, which are required for daylight, color and high acuity vision, also are affected, as are the retina pigmented epithelial (RPE) cells (Chrenek et al., 2012; Napoli et al., 2021; Napoli and Strettoi, 2022; Wu et al., 2021), which support both rod and cone photoreceptors. However, cones and RPE cells typically do not express RP disease genes. Nonetheless, RP cones lose function and die after most of the rods in their immediate neighborhood die. While it is not entirely clear what causes cone death, there are data suggesting problems with metabolism, oxidative stress, lack of trophic factors, oversupply of chromophore, and inflammation (Komeima et al., 2006; Mohand-Said et al., 1998; Punzo et al., 2009; Xue et al., 2023; Zhao et al., 2015). We have been pursuing gene therapy to address some of these problems. Our hope is to create therapies that are disease-gene agnostic by targeting common problems for cones across disease gene families. One of our strategies is aimed at cone metabolism. Several lines of evidence suggest that RP cones do not have enough glucose, their main fuel source (Reviewed in Xue and Cepko 2023). We found that overexpression of Txnip, an α-arrestin protein with multiple functions, including glucose metabolism, prolonged the survival of cones and cone-mediated vision in three RP mouse strains (Xue et al., 2021). Regarding the mechanism of rescue, we found that it relied upon utilization of lactate by cones. In addition, cones treated with Txnip showed improved mitochondrial morphology and function. As Txnip is known to bind directly to thioredoxin, we tested a Txnip allele with a single amino acid (aa) change, C247S, which abolishes the interaction with thioredoxin (Patwari et al., 2006). This allele provided better rescue than the wildtype (wt) Txnip allele, ruling out its interaction with thioredoxin as required for cone rescue. These findings inspired us to further modify Txnip in various ways to look for better rescue, as well as to explore potential mechanisms for Txnip's action. To this end, we also tested a related α-arrestin protein, as well as an interacting partner, for rescue effects.

Results

Arrdc4 reduces *rd1* cone survival

As Txnip is a member of the α-arrestin protein family, we explored whether another family member might prolong RP cone survival. There are six known α-arrestins in mammals (Puca and Brou, 2014). Among them, arrestin domain containing protein 4 (Arrdc4) is the closest to Txnip in amino acid sequence, sharing ~60% similar amino acids with Txnip (**Figure 1A**).Arrdc4 is thought to have functions that are similar to those of Txnip in regulating glucose metabolism *in vitro* (Patwari et

al., 2009). Like Txnip and other α-arrestins, Arrdc4 is composed of three domains: a N-terminal arrestin (Arrestin N-) domain, a C-terminal arrestin (Arrestin C-) domain, and an intrinsically disordered region (IDR) at the C-terminus. Because an IDR lacks a stable 3D structure under physiological conditions, previous studies using crystallography did not reveal the full structure of the TXNIP protein (Hwang et al., 2014). None of the other α-arrestins have been characterized structurally. To begin to examine potential similarities in structure among some of these family members, we utilized an artificial intelligence (AI) algorithm, AlphaFold-2, to visualize the predicted 3D full structure of ARRDC4 (Jumper et al., 2021). Similar to TXNIP, ARRDC4 is predicted to have a "W" shaped arrestin structure, which is composed of the Arrestin N- and C-domains, plus a long IDR which looks like a tail (**Figure 1B**).

Arrdc4 was tested for its ability to prolong cone survival in *rd1* mice using AAV-mediated gene delivery, as was done for Txnip previously (Xue et al., 2021). Expression of Arrdc4 was driven by a cone-specific promoter, RO1.7, derived from human red opsin (Busskamp et al., 2010; Wang et al., 1992; Ye et al., 2016). The vector was packaged into the AAV8 serotype capsid. AAV-Arrdc4 was injected sub-retinally into P0 *rd1* mouse eyes along with AAV-H2BGFP, which is used to trace the infection and to label the cone nuclei for counting. At P50, the treated retinas were harvested and flat-mounted for further quantification of cones within the central retina, the area that first degenerates. Unlike Txnip, the cone counts were much lower in Arrdc4 treated retina relative to the AAV-H2BGFP control (**Figure 1C&D**).

<u>Evaluation of cone survival using Txnip deletion alleles expressed in the RPE</u>

We previously showed (Xue et al., 2021) that overexpressing the Txnip wt allele in the RPE using an RPE-specific promoter, derived from the Best1 gene (Esumi et al., 2009), did not improve RP cone survival. The wt allele removes the glucose transporter from the plasma membrane, thus preventing the RPE from taking up glucose for its own metabolism, and preventing it from serving as a conduit for glucose to flow from the blood to the cones. However, a triple mutant, Txnip.C247S.LL351 and 352AA, improved cone survival when expressed only in the RPE (Xue et al., 2021). The C247S mutation eliminates the interaction with thioredoxin, and enhances the Txnip rescue when expressed in cones (Xue et al., 2021). The LL351 and 352AA mutations eliminate a clathrin-binding site, which is required for Txnip's interaction with clathrin-coated pits for removal of GLUT1 from the cell surface (Wu et al., 2013). We previously proposed a model in which Txnip.C247S.LL351 and 352AA promotes the use of lactate by the RPE (Xue et al., 2021), as we found was the case when Txnip was expressed in cones. Although the RPE normally uses lactate in wt animals, in RP, it is hypothesized that it retains the glucose that it normally would deliver to cones (Reviewed in Hurley 2021). The retention of glucose by the RPE is thought to be due to a reduction in

lactate supply, as rods normally provide lactate for the RPE, and with rod loss that source would be greatly diminished. If the RPE can utilize lactate in RP, perhaps using lactate supplied by the blood, and the LL351 and 352AA mutation impairs the ability of Txnip to remove the glucose transporter from the plasma membrane, this allele of Txnip may then allow glucose to flow from the blood to the cones via the GLUT1 transporter. The expression of Txnip.C247S.LL351 and 352AA allele thus has the potential to address the proposed glucose shortage of RP cones. However, we noted two caveats. One is that survival of cones was not as robust as when Txnip was expressed directly in cones. In addition, the *rd1* retina in the FVB strain used here, even without any treatment, shows holes in the cone layer, which appear as "craters". A RP rat model presents a similar pattern (Ji et al., 2014, 2012; Zhu et al., 2013). When Txnip.C247S.LL351 and 352AA is expressed in the RPE, there are more craters in the photoreceptor layer. We note that these craters are common only in the *rd1* allele on the FVB background, i.e. not as common on other inbred mouse strains that also harbor the *rd1* allele, so the meaning of this observation is unclear.

Arrestins are well-known for their protein-protein interactions via different domains. Different regions of Txnip are known to physically bind to different protein partners to affect several different functions. For example, the N-terminus is sufficient to interact with KPNA2 for Txnip's localization to the nucleus (Nishinaka et al., 2004), while the C-terminus of Txnip is critical for interactions with COPS5, to inhibit cancer cell proliferation (Jeon et al., 2005). The C-terminus of Txnip is also necessary for inhibition of glycolysis, at least *in vitro,* through an unclear mechanism (Patwari et al., 2009). Based on these studies, we made several deletion alleles of Txnip, and expressed them in the RPE. We assayed their ability to clear GLUT1 from the RPE surface (**Figure 2A**), as well as promote cone survival (**Figure 2B-G**). We focused on the basal surface of the RPE, as it is easier to score than the apical surface, where its processes are intertwined with those of the retina, where GLUT1 is also expressed. The 149-397aa portion of Txnip.C247S (C.Txnip.C247S) had the highest activity for GLUT1 removal from the RPE basal surface *in vivo*, while the 1-228aa portion (N.Txnip) failed to remove GLUT1 (**Figure 2A** and **Figure 2-figure supplement 1**). As predicted by ColabFold, an AI algorithm based on AlphaFold-2 (Mirdita et al., 2022), the Arrestin C-domain, which is part of C.Txnip.C247S, but is not present in the N-domain of Txnip, interacts with the intracellular C-terminal IDR of GLUT1 (**Figure 2-figure supplement 2**). These results are consistent with these predictions, in that the C-terminal portion of Txnip is sufficient to bind and clear GLUT1 from cell surface, while the N-domain is not.

Cone survival was assayed *in vivo* following infection of *rd1* with these missense and deletion alleles at P0 and sacrifice at P50 (**Figure 2B-G**). Similar to Best1-wt Txnip (Xue et al., 2021), Best1-Txnip.C247S did not show significant improvement of cone survival, ruling out the C247S mutation alone as promoting the cone survival by Best1-Txnip.C247S.LL351 and 352AA. In addition, Best1-

N.Txnip (1-228aa) and Best1-sC.Txnip (255-397aa, sC: short C-) failed to improve cone survival. However, Best1-C.Txnip.C247S (149-397aa), Best1-C.Txnip.C247S.LL351 and 352AA (149-397aa), and Best1-nt.Txnp.C247S^{320} (1-320aa, nt: no-tail) promoted significant cone survival compared to the corresponding control retinas. Best1-N.Txnip and Best1-sC.Txnip treated *rd1* retina did not have increased numbers of craters, while all other vectors increased the number of craters. These results suggest that the C-terminal portion of Txnip expressed in the RPE is required for RP cone survival, for a function(s) that is unrelated to the removal of GLUT1, or to the mechanism that leads to an increase in craters.

Evaluation of Txnip deletions for autonomous cone survival

Our previous study used the human red opsin promoter, "RedO", in AAV to drive the expression of Txnip in *rd1* cones, with a low level of expression in some rods. This same strategy was used to evaluate whether the aforementioned deletion alleles of Txnip could prolong cone survival. Neither N.Txnip (1-228aa) nor C.Txnip.C247S (149-397aa) promoted significant improvement in *rd1* cone survival. However, nt.Tnxip.C247S^{301} (1-301aa) and nt.Txnip.C247S^{320} (1-320aa) promoted survival of *rd1* cones: 47% and 63% more cones than the control GFP virus, respectively (**Figure 3A&B**). In comparison, the full-length Txnip.C247S promoted an increase of 97% in cones in our previous study (Xue et al., 2021). These results show that the full-length Txnip provides the most benefit in terms of RP cone survival. To determine if expression of this allele might give increased survival when expressed in both the RPE and in cones, we used a CMV promoter to drive expression, as CMV expresses highly in both cell types (Xiong et al., 2015). CMV-Txnip.C247S provided a 38% rescue (**Figure 3A&C**), which is lower than RedO-Txnip.C247S (97%) alone. These and previous results are summarized in **Figure 4**.

Inhibiting Hsp90ab1 prolongs *rd1* cone survival

To further investigate the potential mechanism(s) of cone survival induced by Txnip, we considered the list of protein interactors that were identified in HEK293 cells using biotinylated protein interaction pull-down assay plus mass spectrometry (Forred et al., 2016). Forred et al. identified a subset of proteins that interact with Txnip.C247S, the mutant that provides better cone rescue than the wt Txnip allele (Xue et al., 2021). As we found that Txnip promotes the use of lactate in cones, and improves mitochondrial morphology and function, we looked for Txnip interactors that are relevant to mitochondria. We identified two candidates, PARP1 and HSP90AB1. PARP1 mutants have been shown to protect mitochondria under stress (Hocsak et al., 2017; Szczesny et al., 2014). Accordingly, in our previous study, we crossed the null PARP1 mice with *rd1* mice, to ask if mitochondrial improvements alone were sufficient to induce cone rescue. We found that it was not. In

our current study, we thus prioritized HSP90AB1 inhibition, which had been shown to improve skeletal muscle mitochondrial metabolism in a diabetes mouse model (Jing et al., 2018).

Three shRNAs targeting different regions of the mRNA of *Hsp90ab1* (shHsp90ab1) were delivered by AAV into the retinas of wt mice. Knock-down was evaluated using an AAV encoding a FLAG-tagged Hsp90ab1 that was co-injected with the AAV-shRNA. All three shRNAs reduced the HSP90AB1-FLAG signal compared to the shNC, the non-targeting control shRNA (**Figure 5A&B**), suggesting that they are able to inhibit the expression of HSP90AB1 protein *in vivo*. The promotion of cone survival was then tested in *rd1* mice using these shRNA constructs. The two shRNAs with the most activity in reducing the FLAG-tagged HSP90AB1 signal, shHsp90ab1$^{(\#a)}$ and shHsp90ab1$^{(\#c)}$, were found to increase the survival of *rd1* cones at P50 (**Figure 5C&D**). To determine if this effect was capable of increasing the Txnip effect, the shRNAs were co-injected with Txnip.C247S. A slight additive effect of shHsp90ab1 and Txnip.C247S was observed (**Figure 5E&F**). We also asked if there might be an effect of the knock-down of *Hsp90ab1* on a *Parp1* loss of function background. We did not observe any rescue effect of the shRNAs on this background (**Figure 5G&H**).

Discussion

In RP, the RPE cells and cones degenerate due to non-autonomous causes after the death of rods. Although the causes of cone death are not entirely clear, one model proposes that they do not have enough glucose, their main fuel source (Hurley, 2021; Punzo et al., 2009; Xue and Cepko, 2023). In a previous study, we found that Txnip promoted the use of lactate within cones and led to healthier mitochondria. The mechanisms for these effects are unclear, and we sought to determine what domains of Txnip might contribute to these effects, as well as explore alleles of Txnip that might be more potent for cone survival. We further tested the rescue effects of several alleles when expressed in the RPE, a support layer for cones, through which nutrients, such as glucose, flow to the cones from the choriocapillaris. The results suggest that Txnip has different mechanisms for Txnip-mediated cone survival when expressed in the RPE versus in cones.

The C-terminal portion of Txnip.C247S (149-397aa) expressed within the RPE, but not within cones, delayed the degeneration of cones (**Figure 2**). The full length Txnip.C247S expressed within cones, but not within the RPE, was the most effective configuration for cone survival (**Figure 3**). The expression of full length Txnip.C247S in both the RPE and cones did not provide better rescue than in cones alone. As Txnip has several domains that presumably interact with different partners, it is possible that these different effects on cone survival are due to the interaction of different Txnip domains with different partners in the RPE versus the cones, or different results from the interactions

of the same domains and partners in the two cell types. The N-terminal half of Txnip (1-228aa) might exert harmful effects in the RPE, that negate the beneficial effects from the C-terminal half, suggested by the observation that its removal, in the C-terminal 149-397 allele, led to better cone survival when expressed in the RPE (**Figure 2**). In cones, the C-terminal half, including the C-terminal IDR tail, may cooperate with the N-terminal half, or negate its negative effects, to benefit RP cone survival. However, the C-terminal half is not sufficient for cone rescue when expressed in cones, as the 149-397 allele did not rescue.

The C-terminal half of Txnip apparently affects cone survival differently when expressed within the two cell types. This notion is informed by the different rescue effects of expression of the 149-397 allele, which rescues cones when expressed in the RPE, but not when expressed in cones. This domain loses the cone rescue activity if it loses aa 149-254, when expressed in the RPE, as shown by the 255-397 allele. In cones, the rescue activity is present in the 1-301 and the 1-320 allele, but is lost in the 149-397 allele. It is possible that effects on protein structure cause this loss, or that an interaction between N-terminal and C-terminal domains is required for cone rescue within cones.

One Txnip function that likely is important to these effects in the two cell types is Txnip's removal of the glucose transporter from the plasma membrane. The LLAA Txnip mutant is unable to effectively remove the transporter, due to its loss of interaction with clathrin (Wu et al., 2013). When this mutant allele is expressed in the RPE, it leads to improved cone survival, in contrast to the wt allele. This might be due to better health in the RPE, when it is able to take up glucose to fuel its own metabolism, and/or to provide glucose to cones. When the LLAA allele is expressed in cones, it also promotes cone survival, though not as well as the wt allele (Xue et al., 2021). The wt allele might be more beneficial in cones if it is part of the mechanism that forces cones to rely more heavily on lactate vs. glucose. All of these observations of cone rescue from expression within cones suggest that cone rescue relies on activities that reside in both the N and C-terminal portions, including the ability of Txnip to interact with clathrin. However, it will be important to probe structural alterations and stability of Txnip in cones and RPE when these various alleles are expressed to further support these hypotheses.

Arrdc4, the most similar α-arrestin protein to Txnip that also has Arrestin N- and C- domains, accelerated RP cone death when transduced via AAV (**Figure 1**). This observation suggests that Txnip has unique functions that protect RP cones. Recently, Arrdc4 has been proposed to be critical for liver glucagon signaling, which could be negated by insulin (Dagdeviren et al., 2023). The implication of this potential role regarding RP cone survival is unclear, but interestingly, the activation of the insulin/mTORC1 pathway is beneficial to RP cone survival (Punzo et al., 2009; Venkatesh et al., 2015).

Regarding potential protein interactions beyond the glucose transporter, the interaction of Txnip with thioredoxin is apparently negative for cone survival, as we found in our previous study with the C247S allele. This is most easily understood by the release of thioredoxin from Txnip, whereupon it can play its anti-oxidation role, which would be important in the RP retina which exhibits oxidative damage. It also would free Txnip to interact with other partners, of which there are several, though many also depend upon C247 (Forred et al., 2016). Another partner interaction suggested by previous studies and explored here is the interaction with HSP90AB1 (**Figure 5**). HSP90AB1 interacts with both the wt and C247S alleles (Forred et al., 2016). Little is known about the function of HSP90AB1. Knocking down *Hsp90ab1* improved mitochondrial metabolism of skeletal muscle in a diabetic mouse model (Jing et al., 2018). Knocking out HSP90AA1, a paralog of HSP90AB1 which has 14% different amino acids, led to rod death and correlated with PDE6 dysregulation (Munezero et al., 2023). Inhibiting HSP90AA1 with small molecules transiently delayed cone death in human retinal organoids under low glucose conditions (Spirig et al., 2023). However, the exact role of HSP90AA1 in photoreceptors needs to be clarified, and the implications for HSP90AB1 in RP cones are still unclear.

Here we found that sh-mediated knock-down of *Hsp90ab1* enhanced cone survival in *rd1* mice. This rescue seems to be dependent on PARP1, another binding partner of wt Txnip and Txnip.C247S (Forred et al., 2016). As shown by PARP1 knock out mice, PARP1 is deleterious to mitochondrial heath under stressful conditions (Hocsak et al., 2017; Szczesny et al., 2014; Xue et al., 2021). When we examined a possible rescue effect of PARP1 loss on *rd1* cone survival, we did not see a benefit, indicating that the Txnip-mediated rescue is not due solely to its beneficial effects on mitochondria, nor does Txnip-mediated rescue rely upon PARP1 (Xue et al., 2021). These results indicate that the Txnip rescue is more complex than inhibition of HSP90AB1, and a PARP1-independent mechanism is involved. It is possible that HSP90AB1 directly interacts with PARP1, and this interaction is critical for shHsp90ab1 to benefit RP cones. We looked into the predicted 3D structures of HSP90AB1 and PARP1 using AlphaFold-2 (**Figure 5-figure supplement 1**), but did not gain additional insight into such interactions. We also explored AlphaFold Multimer, which is an algorithm predicting the interaction of multiple proteins based upon AlphaFold-2 (Evans et al., 2021), and noticed that the Arrestin-C domain of Txnip linked PARP1 and HSP90AB1 together in one of the predicted models (**Figure 5-figure supplement 2**). Despite the unclear mechanism, combining Hsp90ab1 inhibition with Txnip.C247S could be a potential combination therapy to maximize the protection of RP cones.

Material and Methods

Key Resources Table				
Reagent type (species) or resource	**Designation**	**Source or reference**	**Identifiers**	**Additional information**
Antibody	Rabbit anti-GLUT1	Abcam	ab115730	IHC (1:500)
Genetic reagent (M. musculus)	Arrdc4 cDNA	GeneCopoeia	Cat. #: Mm26972 NCBI: NM_001042592.2	
Genetic reagent (M. musculus)	Hsp90ab1 cDNA	GeneCopoeia	Cat. #: Mm03161 NCBI: NM_008302.3	
software, algorithm	Protein 3D structure prediction	AlphaFold-2	TXNIP (M. musculus); ARRDC4 (M. musculus); HSP90AB1 (M. musculus); PARP1 (M. musculus)	(Jumper et al., 2021) https://alphafold.ebi.ac.uk
software, algorithm	Protein 3D interaction prediction	ColabFold	AlphaFold2_mmseqs2	(Mirdita et al., 2022) https://github.com/sokrypton/colabfold
software, algorithm	Protein 3D interaction prediction	COSMIC2	AlphaFold2 – Multimer	(Evans et al., 2021) http://cosmic-cryoem.org/tools/alphafoldmultimer/
software, algorithm	Protein 3D structure viewer	RCSB PDB	Mol* 3D Viewer	To visualize the 3D structure of proteins in .pdb files https://www.rcsb.org/3d-view

The material and methods in this study are similar to those used in our previous study (Xue et al., 2021). The cone number of the central retina is defined as the counts of H2BGFP-positive cells within the central portion of the retina. New reagents and algorithms used in this study are listed in the Key resources table above. Txnip deletions were cloned from the Txnip plasmid using Gibson assembly (**Figure 4**). The following sense strand sequences were used to knock down the Hsp90ab1: shHsp90ab1(#a) 5′ - GCATCTACCGCATGATTAAAC-3′ ; shHsp90ab1(#b) 5′ - CCAGAAGTCCATCTACTATAT-3′ ; shHsp90ab1(#c) 5′ - CCTGAGTACCTCAACTTTATC-3′ . For RPE basal surface GLUT1 quantification, multiple regions of interest (ROI) were selected from at

least three eyes of each condition, and the mean intensity of the ROI was measured using ImageJ software. Statistics are listed in each figure legend.

Acknowledgments

We thank John Dingus, Sophia Zhao, and Paula Montero-Llopis (Microscopy Resources on the North Quad) of Harvard Medical School, Xiaomei Sun and Peimin Ma of Lingang Laboratory, Li Tan and Kangning Sang (Optical Imaging Core Facility) of Shanghai Research Center for Brain Science and Brain-Inspired Intelligence for advisory and technical support. This work was funded by Howard Hughes Medical Institute (to C.L.C.), National Institutes of Health (NIH) grants K99EY030951 (to Y.X. before June 30, 2022), Lingang Laboratory startup fund (to Y.X. after July 20, 2022).

References

Busskamp V, Duebel J, Balya D, Fradot M, Viney TJ, Siegert S, Groner AC, Cabuy E, Forster V, Seeliger M, Biel M, Humphries P, Paques M, Mohand-Said S, Trono D, Deisseroth K, Sahel JA, Picaud S, Roska B. 2010. Genetic Reactivation of Cone Photoreceptors Restores Visual Responses in Retinitis Pigmentosa. *Science (80-)* **329**:413–417. doi:10.1126/science.1190897

Chrenek MA, Dalal N, Gardner C, Grossniklausgrossniklaus H, Jiang Y, Boatright JH, Nickerson JM. 2012. Analysis of the RPE sheet in the rd10 retinal degeneration model. *Adv Exp Med Biol* **723**:641–647. doi:10.1007/978-1-4614-0631-0_81

Dagdeviren S, Hoang MF, Sarikhani M, Meier V, Benoit JC, Okawa MC, Melnik VY, Ricci-Blair EM, Foot N, Friedline RH, Hu X, Tauer LA, Srinivasan A, Prigozhin MB, Shenoy SK, Kumar S, Kim JK, Lee RT. 2023. An insulin-regulated arrestin domain protein controls hepatic glucagon action. *J Biol Chem* **299**. doi:10.1016/J.JBC.2023.105045

Esumi N, Kachi S, Hackler L, Masuda T, Yang Z, Campochiaro PA, Zack DJ. 2009. BEST1 expression in the retinal pigment epithelium is modulated by OTX family members. *Hum Mol Genet* **18**:128–141. doi:10.1093/hmg/ddn323

Evans R, O'Neill M, Pritzel A, Antropova N, Senior A, Green T, Žídek A, Bates R, Blackwell S, Yim J, Ronneberger O, Bodenstein S, Zielinski M, Bridgland A, Potapenko A, Cowie A, Tunyasuvunakool K, Jain R, Clancy E, Kohli P, Jumper J, Hassabis D. 2021. Protein complex prediction with AlphaFold-Multimer. *bioRxiv* 2021.10.04.463034. doi:10.1101/2021.10.04.463034

Forred BJ, Neuharth S, Kim DI, Amolins MW, Motamedchaboki K, Roux KJ, Vitiello PF. 2016. Identification of Redox and Glucose-Dependent Txnip Protein Interactions. *Oxid Med Cell Longev* **2016**. doi:10.1155/2016/5829063

Hartong DT, Berson EL, Dryja TP. 2006. Retinitis pigmentosa. *Lancet* **368**:1795–809. doi:10.1016/S0140-6736(06)69740-7

Hocsak E, Szabo V, Kalman N, Antus C, Cseh A, Sumegi K, Eros K, Hegedus Z, Gallyas F, Sumegi B, Racz B. 2017. PARP inhibition protects mitochondria and reduces ROS production via PARP-1-ATF4-MKP-1-MAPK retrograde pathway. *Free Radic Biol Med* **108**:770–784. doi:10.1016/j.freeradbiomed.2017.04.018

Hurley JB. 2021. Retina Metabolism and Metabolism in the Pigmented Epithelium: A Busy Intersection. *Annu Rev Vis Sci* **7**:665. doi:10.1146/ANNUREV-VISION-100419-115156

Hwang J, Suh HW, Jeon YH o., Hwang E, Nguyen LT, Yeom J, Lee SG, Lee C, Kim KJ i., Kang BS i., Jeong JO, Oh TK, Choi I, Lee JO, Kim MH e. 2014. The structural basis for the negative regulation of thioredoxin by thioredoxin-interacting protein. *Nat Commun* **5**:2958. doi:10.1038/ncomms3958

Jeon JH, Lee KN, Hwang CY, Kwon KS, You KH, Choi I. 2005. Tumor suppressor VDUP1 increases p27(kip1) stability by inhibiting JAB1. *Cancer Res* **65**:4485–4489. doi:10.1158/0008-5472.CAN-04-2271

Ji Y, Yu WQ, Eom YS, Bruce F, Craft CM, Grzywacz NM, Lee EJ. 2014. The effect of TIMP-1 on the cone mosaic in the retina of the rat model of retinitis pigmentosa. *Invest Ophthalmol Vis Sci* **56**:352–364. doi:10.1167/IOVS.14-15398

Ji Y, Zhu CL, Grzywacz NM, Lee EJ. 2012. Rearrangement of the cone mosaic in the retina of the rat model of retinitis pigmentosa. *J Comp Neurol* **520**:874–888. doi:10.1002/cne.22800

Jing E, Sundararajan P, Majumdar ID, Hazarika S, Fowler S, Szeto A, Gesta S, Mendez AJ, Vishnudas VK, Sarangarajan R, Narain NR. 2018. Hsp90β knockdown in DIO mice reverses insulin resistance and improves glucose tolerance. *Nutr Metab (Lond)* **15**. doi:10.1186/S12986-018-0242-6

Jumper J, Evans R, Pritzel A, Green T, Figurnov M, Ronneberger O, Tunyasuvunakool K, Bates R, Žídek A, Potapenko A, Bridgland A, Meyer C, Kohl SAA, Ballard AJ, Cowie A, Romera-Paredes B, Nikolov S, Jain R, Adler J, Back T, Petersen S, Reiman D, Clancy E, Zielinski M, Steinegger M, Pacholska M, Berghammer T, Bodenstein S, Silver D, Vinyals O, Senior AW, Kavukcuoglu K, Kohli P, Hassabis D. 2021. Highly accurate protein structure prediction with AlphaFold. *Nature* **596**:583–589. doi:10.1038/S41586-021-03819-2

Komeima K, Rogers BS, Lu L, Campochiaro PA. 2006. Antioxidants reduce cone cell death in a model of retinitis pigmentosa. *Proc Natl Acad Sci U S A* **103**:11300–11305. doi:10.1073/pnas.0604056103

Mirdita M, Schütze K, Moriwaki Y, Heo L, Ovchinnikov S, Steinegger M. 2022. ColabFold: making protein folding accessible to all. *Nat Methods* **19**:679–682. doi:10.1038/S41592-022-01488-1

Mohand-Said S, Deudon-Combe A, Hicks D, Simonutti M, Forster V, Fintz AC, Léveillard T, Dreyfus H, Sahel JA. 1998. Normal retina releases a diffusible factor stimulating cone survival in the retinal degeneration mouse. *Proc Natl Acad Sci U S A* **95**:8357–8362. doi:10.1073/PNAS.95.14.8357

Munezero D, Aliff H, Salido E, Saravanan T, Sanzhaeva U, Guan T, Ramamurthy V. 2023. HSP90α is needed for the survival of rod photoreceptors and regulates the expression of rod PDE6 subunits. *J Biol Chem* **299**. doi:10.1016/J.JBC.2023.104809

Napoli D, Biagioni M, Billeri F, Marco B Di, Orsini N, Novelli E, Strettoi E. 2021. Retinal Pigment Epithelium Remodeling in Mouse Models of Retinitis Pigmentosa. *Int J Mol Sci* **22**. doi:10.3390/IJMS22105381

Napoli D, Strettoi E. 2022. Structural abnormalities of retinal pigment epithelial cells in a light-inducible, rhodopsin mutant mouse. *J Anat*. doi:10.1111/joa.13667

Nishinaka Y, Masutani H, Oka SI, Matsuo Y, Yamaguchi Y, Nishio K, Ishii Y, Yodoi J. 2004. Importin alpha1 (Rch1) mediates nuclear translocation of thioredoxin-binding protein-2/vitamin D(3)-up-regulated protein 1. *J Biol Chem* **279**:37559–37565. doi:10.1074/JBC.M405473200

Patwari P, Chutkow WA, Cummings K, Verstraeten VLRM, Lammerding J, Schreiter ER, Lee RT. 2009. Thioredoxin-independent regulation of metabolism by the α-arrestin proteins. *J Biol Chem* **284**:24996–25003. doi:10.1074/jbc.M109.018093

Patwari P, Higgins LJ, Chutkow WA, Yoshioka J, Lee RT. 2006. The interaction of thioredoxin with Txnip: Evidence for formation of a mixed disulfide by disulfide exchange. *J Biol Chem* **281**:21884–21891. doi:10.1074/jbc.M600427200

Puca L, Brou C. 2014. α-Arrestins - new players in Notch and GPCR signaling pathways in mammals. *J Cell Sci*. doi:10.1242/jcs.142539

Punzo C, Kornacker K, Cepko CL. 2009. Stimulation of the insulin/mTOR pathway delays cone death in a mouse model of retinitis pigmentosa. *Nat Neurosci* **12**:44–52. doi:10.1038/nn.2234

Spirig SE, Arteaga-Moreta VJ, Raics Z, Posada-Céspedes S, Chreng S, Galuba O, Galuba I, Claerr I, Renner S, Kleindienst PT, Volak A, Imbach J, Malysheva S, Siwicki RA, Hahaut V, Hou Y, Picelli S, Cattaneo M, Jüttner J, Cowan CS, Duckely M, Baeschlin DK, Renner M, Unterreiner V, Roska B. 2023. Cell type-focused compound screen in human organoids reveals molecules and pathways controlling cone photoreceptor death. *bioRxiv* 2023.10.09.561525. doi:10.1101/2023.10.09.561525

Szczesny B, Brunyanszki A, Olah G, Mitra S, Szabo C. 2014. Opposing roles of mitochondrial and nuclear PARP1 in the regulation of mitochondrial and nuclear DNA integrity: Implications for the regulation of mitochondrial function. *Nucleic Acids Res* **42**:13161–13173. doi:10.1093/nar/gku1089

Venkatesh A, Ma S, Le YZ, Hall MN, Rüegg MA, Punzo C. 2015. Activated mTORC1 promotes long-term cone survival in retinitis pigmentosa mice. *J Clin Invest* **125**:1446–58. doi:10.1172/JCI79766

Wang Y, Macke JP, Merbs SL, Zack DJ, Klaunberg B, Bennett J, Gearhart J, Nathans J. 1992. A locus control region adjacent to the human red and green visual pigment genes. *Neuron* **9**:429–440. doi:10.1016/0896-6273(92)90181-C

Wu DM, Ji X, Ivanchenko M V., Chung M, Piper M, Rana P, Wang SK, Xue Y, West E, Zhao SR, Xu H, Cicconet M, Xiong W, Cepko CL. 2021. Nrf2 overexpression rescues the RPE in mouse models of retinitis pigmentosa. *JCI Insight* **6**. doi:10.1172/jci.insight.145029

Wu N, Zheng B, Shaywitz A, Dagon Y, Tower C, Bellinger G, Shen C-H, Wen J, Asara J, McGraw TE, Kahn BB, Cantley LC. 2013. AMPK-dependent degradation of TXNIP upon energy stress leads to enhanced glucose uptake via GLUT1. *Mol Cell* **49**:1167–75. doi:10.1016/j.molcel.2013.01.035

Xiong W, MacColl Garfinkel AE, Li Y, Benowitz LI, Cepko CL. 2015. NRF2 promotes neuronal survival in neurodegeneration and acute nerve damage. *J Clin Invest* **125**:1433–45. doi:10.1172/JCI79735

Xue Y, Cepko CL. 2023. Gene Therapies for Retinitis Pigmentosa that Target Glucose Metabolism In: Banin E, Bennett J, Duncan JL, Roska B, Sahel J-A, editors. Retinal Disorders: Genetic Approaches to Diagnosis and Treatment. Cold Spring Harbor Laboratory Press.

Xue Y, Sun X, Wang SK, Collin GB, Kefalov VJ, Cepko CL. 2023. Chromophore supply modulates cone function and survival in retinitis pigmentosa mouse models. *Proc Natl Acad Sci U S A* **120**. doi:10.1073/PNAS.2217885120

Xue Y, Wang SK, Rana P, West ER, Hong CM, Feng H, Wu DM, Cepko CL. 2021. AAV-Txnip prolongs cone survival and vision in mouse models of retinitis pigmentosa. *Elife* **10**. doi:10.7554/eLife.66240

Ye GJ, Budzynski E, Sonnentag P, Nork TM, Sheibani N, Gurel Z, Boye SL, Peterson JJ, Boye SE, Hauswirth WW, Chulay JD. 2016. Cone-Specific Promoters for Gene Therapy of Achromatopsia and Other Retinal Diseases. *Hum Gene Ther* **27**:72–82. doi:10.1089/hum.2015.130

Zhao L, Zabel MK, Wang X, Ma W, Shah P, Fariss RN, Qian H, Parkhurst CN, Gan W, Wong WT. 2015. Microglial phagocytosis of living photoreceptors contributes to inherited retinal degeneration. *EMBO Mol Med* **7**:1179–1197. doi:10.15252/emmm.201505298

Zhu CL, Ji Y, Lee EJ, Grzywacz NM. 2013. Spatiotemporal pattern of rod degeneration in the S334ter-line-3 rat model of retinitis pigmentosa. *Cell Tissue Res* **351**:29–40. doi:10.1007/S00441-012-1522-5

Figure 1 Effect of Arrdc4 on cone survival in retinitis pigmentosa (RP) mice.

A. Amino acid sequences of mouse TXNIP and mouse ARRDC4. In the full length alignment (421 amino acid), Identity: 172 / 421, 40.86%; Similarity: 246 / 421, 58.43%; Gaps: 28 / 421, 6.65%. Color code: identical, black; similar, blue; not similar, red.

B. Predicted 3D protein structures of mouse TXNIP and mouse ARRDC4 by artificial intelligence (AI) algorithm AlphaFold-2. Abbreviations: Arr N-, N-terminal arrestin domain; Arr C-, C-terminal arrestin domain.

C. Representative P50 *rd1* flat-mounted retinas after P0 subretinal infection with AAV8-RO1.7-Arrdc4 (1×10^9 vg/eye), plus AAV8-RedO-H2BGFP (2.5×10^8 vg/eye), or control eyes infected with AAV8-RedO-H2BGFP, 2.5×10^8 vg/eye alone.

D. Quantification of H2BGFP-positive cones within the center of P50 *rd1* retinas transduced with Arrdc4, and control (same as in C). The number in the round brackets '()' indicates the number of retinas within each group. Error bar: standard deviation. Statistics: two-tailed unpaired Student's t-test. **** p< or <<0.0001.

RedO: red opsin promoter; RO1.7: a 1.7kb version of red opsin promoter. AAV: adeno-associated virus.

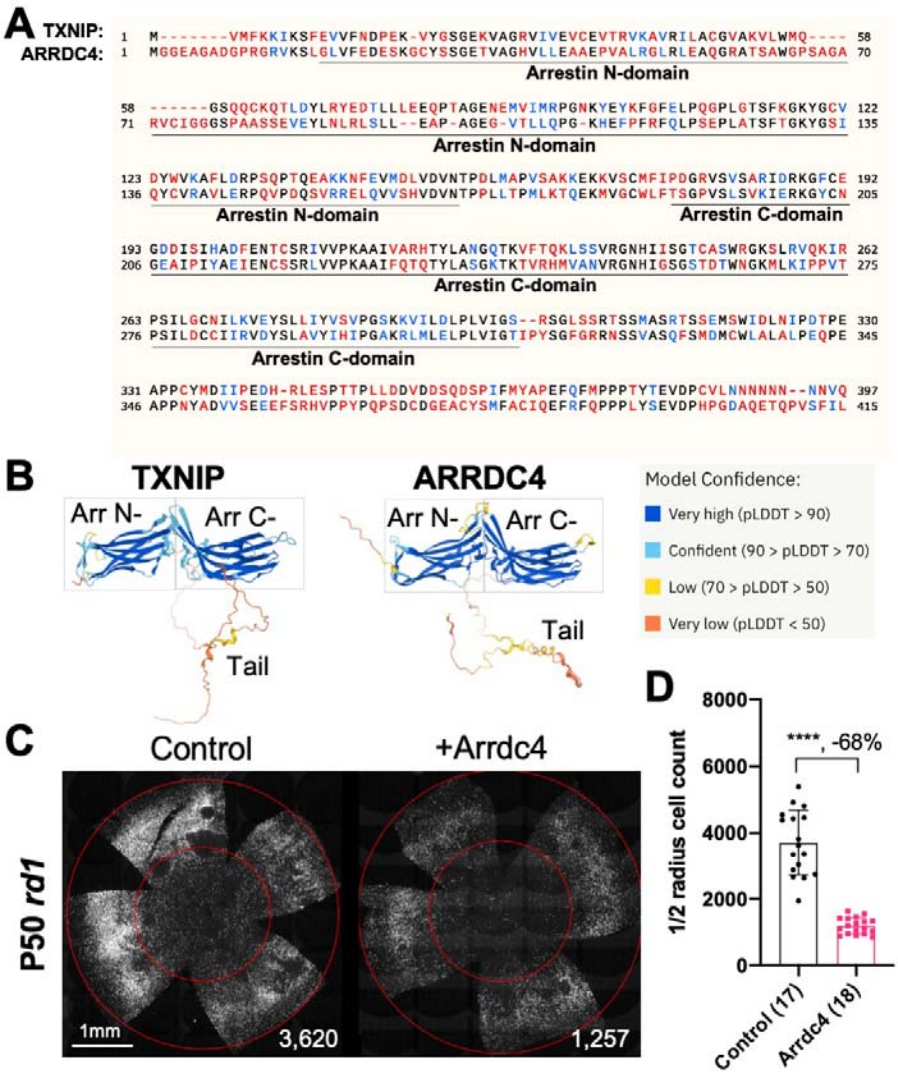
A
TXNIP:
ARRDC4:
Arrestin N-domain
Arrestin C-domain
B
TXNIP
ARRDC4
Arr N-
Arr C-
Tail
Model Confidence:
Very high (pLDDT > 90)
Confident (90 > pLDDT > 70)
Low (70 > pLDDT > 50)
Very low (pLDDT < 50)
C
Control
+Arrdc4
P50 rd1
1mm
3,620
1,257
D
1/2 radius cell count
****, -68%
Control (17)
Arrdc4 (18)

Figure 1

Figure 2 Txnip deletions expressed only within RPE cells: effects on GLUT1 removal and cone survival.

A. Glucose transporter 1 (GLUT1) expression in P20 wildtype eyes infected with control (AAV8-RedO-H2BGFP, 2.5×10^8 vg/eye), or a Txnip allele (2.5×10^8 vg/eye) plus RedO-H2BGFP (2.5×10^8 vg/eye), as indicated in each panel. Txnip deletions are detailed in **Figure 4**. GLUT1 intensity from basal RPE is quantified in **Figure 2-figure supplement 1**. Magenta: GLUT1; green: RedO-H2BGFP for infection tracing; gray: DAPI.

B, D, F. Representative P50 *rd1* flat-mounted retinas after P0 infection with one of seven different Txnip alleles expressed only within the RPE, as indicated in the figure, or control eyes infected with AAV8-RedO-H2BGFP, 2.5×10^8 vg/eye alone.

C, E, G. Quantification of H2BGFP-positive cones within the center of P50 *rd1* retinas transduced with indicated vectors, as shown in B, D, F. The number in the round brackets '()' indicates the number of retinas within each group. Error bar: standard deviation. Statistics: ANOVA and Dunnett's multiple comparison test for C and E; two-tailed unpaired Student's t-test for G.

C.Txnip.CS: C-terminal portion of Txnip.C247S; C.Txnip.CS.LLAA: C-terminal portion of Txnip.C247S.LL351 and 352AA; nt.Txnip.CS^{320}: no tail Txnip (1-320aa). NS: not significant, $p>0.05$, *$p<0.05$, **$p<0.01$, **** p< or <<0.0001. Best1: Best1 promoter.

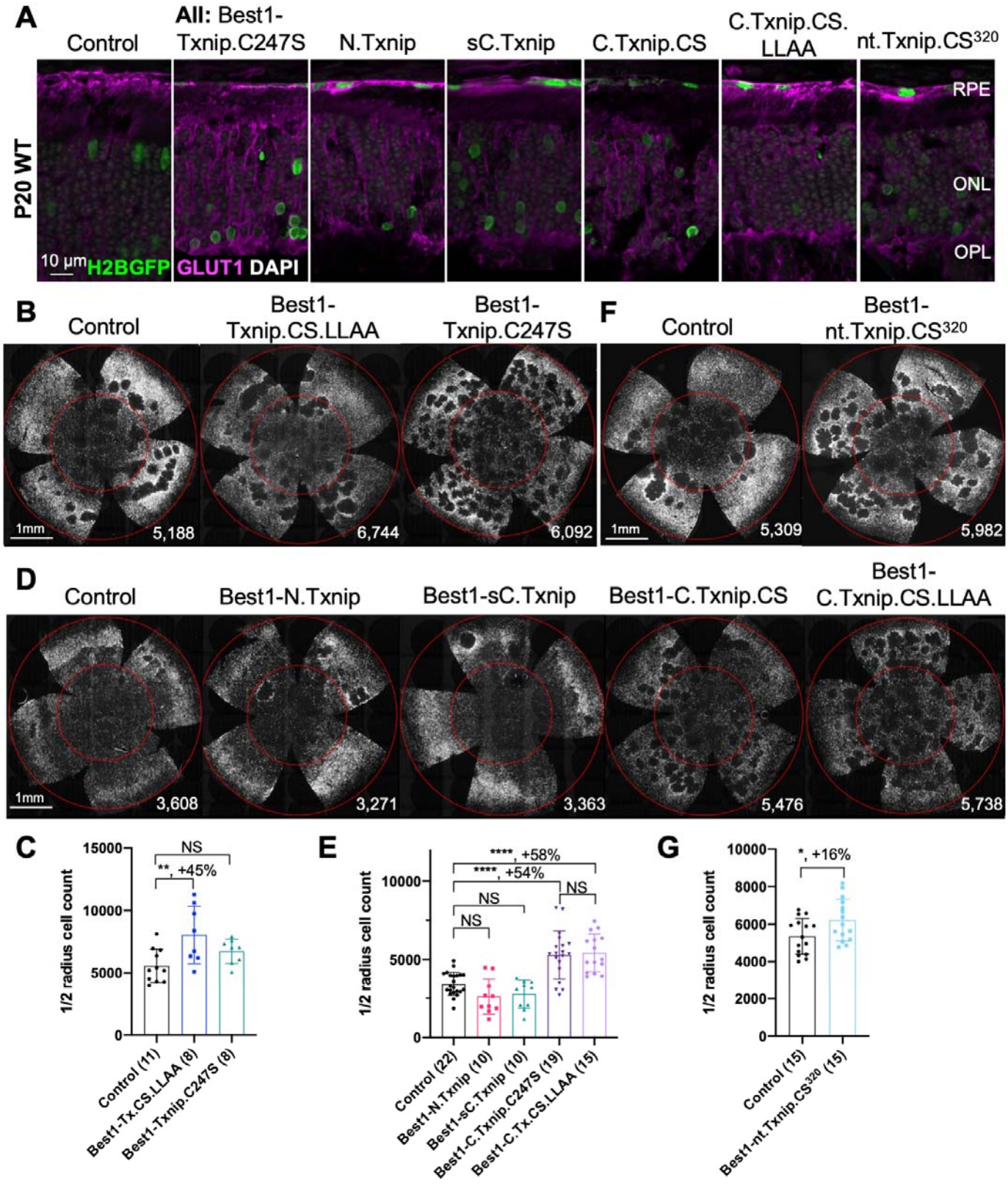
A
Control
All: Best1-Txnip.C247S
N.Txnip
sC.Txnip
C.Txnip.CS
C.Txnip.CS. LLAA
nt.Txnip.CS320
P20 WT
RPE
ONL
OPL
10 µm
H2BGFP
GLUT1
DAPI
B
Control
Best1-Txnip.CS.LLAA
Best1-Txnip.C247S
1mm
5,188
6,744
6,092
F
Control
Best1-nt.Txnip.CS320
1mm
5,309
5,982
D
Control
Best1-N.Txnip
Best1-sC.Txnip
Best1-C.Txnip.CS
Best1-C.Txnip.CS.LLAA
1mm
3,608
3,271
3,363
5,476
5,738
C
1/2 radius cell count
NS
**, +45%
Control (11)
Best1-Tx.CS.LLAA (8)
Best1-Txnip.C247S (8)
E
1/2 radius cell count
****, +58%
****, +54%
NS
Control (22)
Best1-N.Txnip (10)
Best1-sC.Txnip (10)
Best1-C.Txnip.C247S (19)
Best1-C.Tx.CS.LLAA (15)
G
1/2 radius cell count
*, +16%
Control (15)
Best1-nt.Txnip.CS320 (15)

Figure 2

Figure 2-figure supplement 1 Txnip deletions expressed only within RPE cells: quantification of the GLUT1 level within the basal surface of the RPE. GLUT1 expression in P20 wt eyes infected with control (AAV8-RedO-H2BGFP, 2.5×10^8 vg/eye), or a Txnip allele (2.5×10^8 vg/eye) plus RedO-H2BGFP (2.5×10^8 vg/eye), as indicated in each panel. Txnip deletions are detailed in **Figure 4**. Wt Txnip (red group) and Txnip.C247S.LLAA (blue group) were published previously (Xue et al., 2021), and are repeated here using the same conditions as in this study for comparison to the new alleles. Only regions that were infected, as indicated by the H2BGFP marker that was co-injected, were analyzed. GLUT1 intensity from regions of interest (ROIs) within the basal RPE was quantified. Red: GLUT1; green: RedO-H2BGFP for infection tracing; gray: DAPI. Arrows: RPE basal surface. Sample size: control, 26 ROIs from 4 eyes; Txnip.C247S, 9 ROIs from 3 eyes; N.Txnip, 36 ROIs from 6 eyes; sC.Txnip, 10 ROIs from 6 eyes; C.Txnip.CS, 13 ROIs from 3 eyes, C.Txnip.CS.LLAA, 7 ROIs from 3 eyes; nt.Tnip.CS^{320}, 14 ROIs from 4 eyes; wt Txnip, 11 ROIs from 4 eyes; Txnip.CS.LLAA, 21 ROIs from 4 eyes. Error bar: standard deviation. Statistics: Mann-Whitney U Test compared to control with Bonferroni correction. NS: not significant, *** $p<0.001$, **** $p<$ or $<<0.0001$.

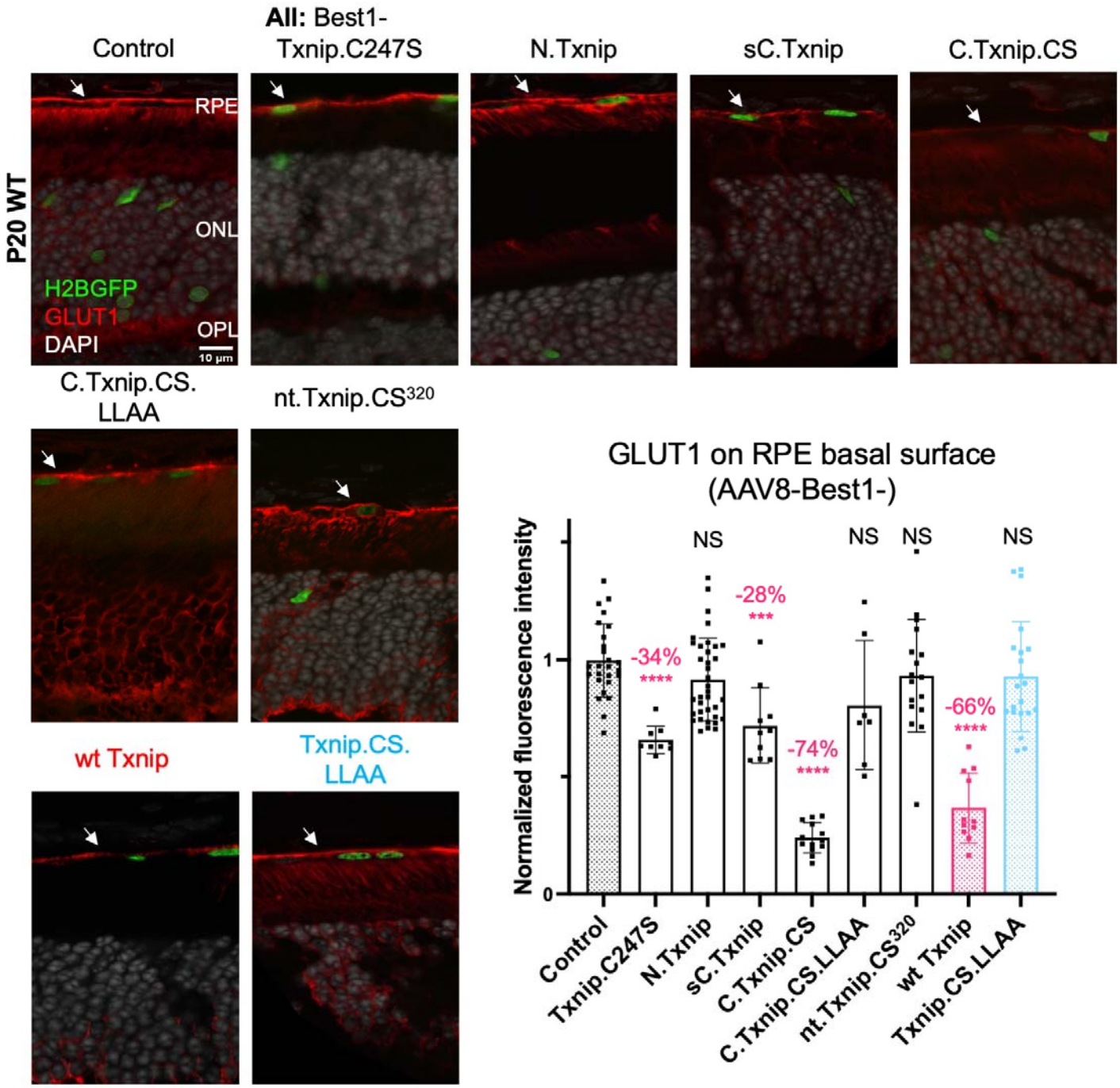

Figure 2 Supplement 1

Figure 2-figure supplement 2 Predicted protein-protein interactions of TXNIP and GLUT1 by an algorithm, ColabFold, based on AlphaFold-2.

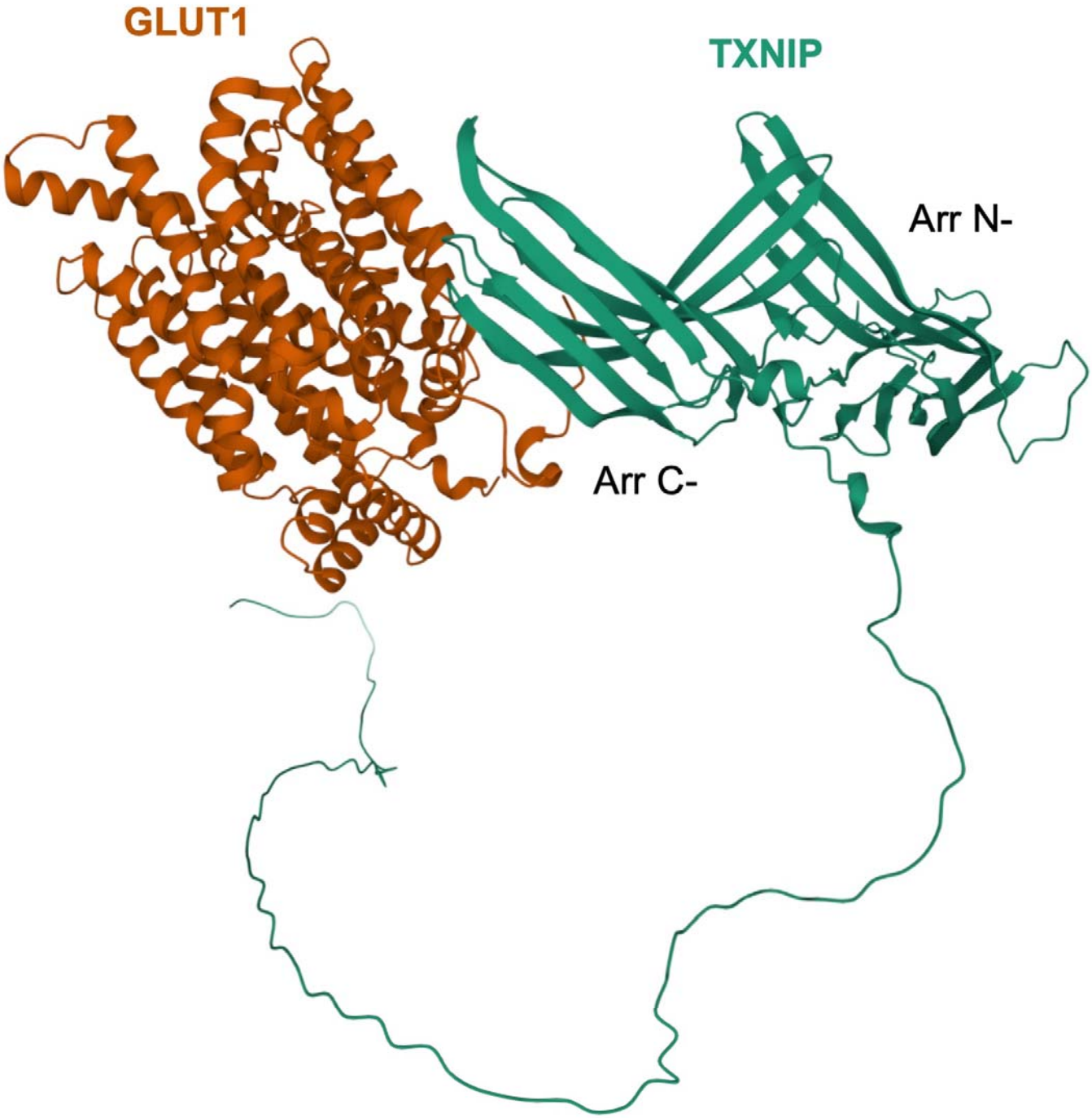

Figure 2 Supplement 2

Figure 3 Tests of Txnip alleles on cone survival.

A. Representative P50 *rd1* flat-mounted retinas after P0 infection with one of 5 different Txnip alleles (AAV8-RedO- N.Txnip /C.Txnip.C247S/ nt.Txnip.C247S$^{1\text{-}301}$/nt.Txnip.C247S$^{1\text{-}320}$ or AAV8-CMV-Txnip.C247S, ≈1 × 10^9 vg/eye, plus AAV8-RedO-H2BGFP, 2.5 × 10^8 vg/eye), or control eyes infected with AAV8-RedO-H2BGFP, 2.5 × 10^8 vg/eye alone.

B, C. Quantification of H2BGFP-positive cones within the center of P50 *rd1* retinas transduced with AAV8-RedO- N.Txnip /C.Txnip.C247S/ nt.Txnip.C247S$^{1\text{-}301}$/nt.Txnip.C247S$^{1\text{-}320}$ or AAV8-CMV-Txnip.C247S, and control (same as in A). The number in the round brackets '()' indicates the number of retinas within each group. Error bar: standard deviation. Statistics: ANOVA and Dunnett's multiple comparison test for B; two-tailed unpaired Student's t-test for C. NS: not significant, **** p< or <<0.0001.

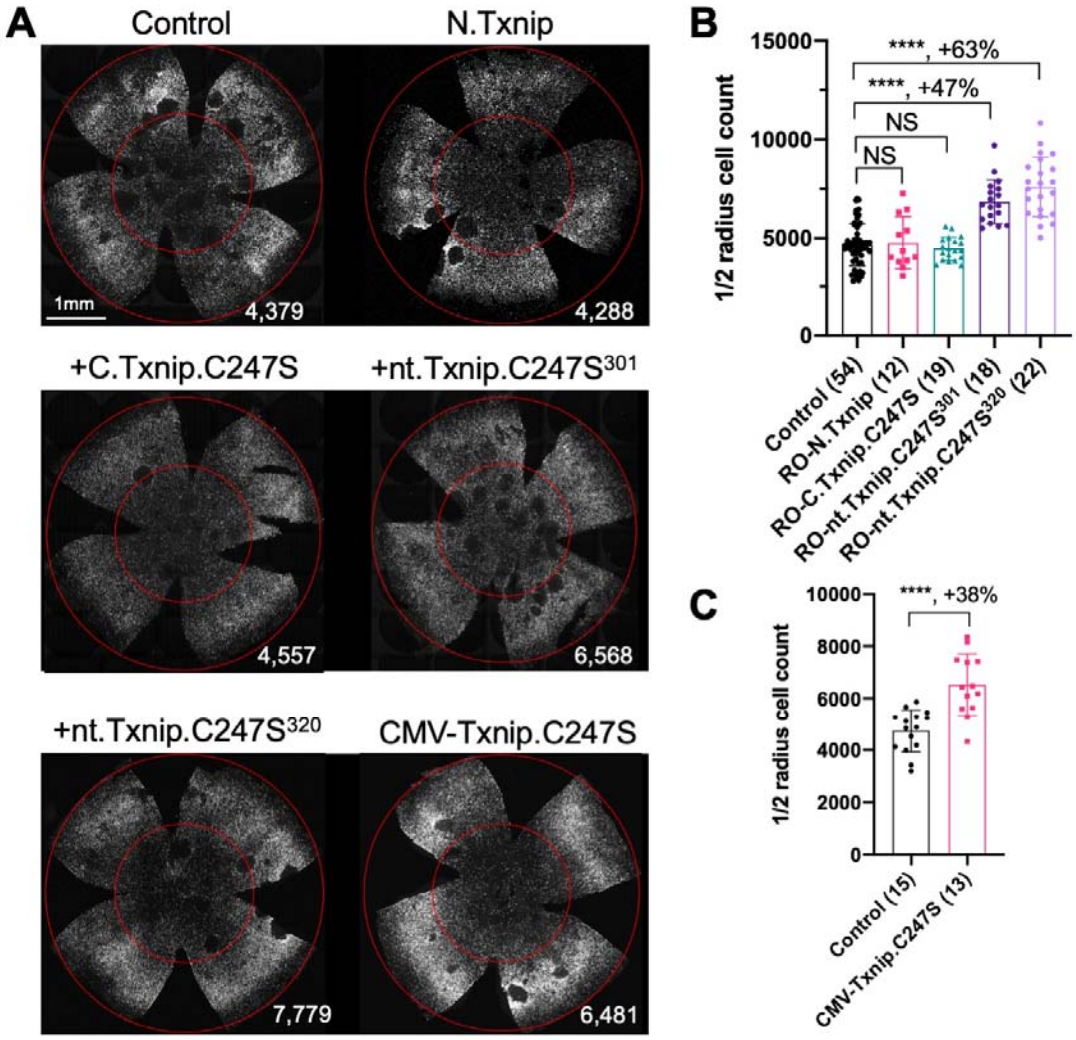
A
Control
N.Txnip
1mm
4,379
4,288
+C.Txnip.C247S
+nt.Txnip.C247S301
4,557
6,568
+nt.Txnip.C247S320
CMV-Txnip.C247S
7,779
6,481
B
1/2 radius cell count
15000
10000
5000
0
****, +63%
****, +47%
NS
NS
Control (54)
RO-N.Txnip (12)
RO-C.Txnip.C247S (19)
RO-nt.Txnip.C247S301 (18)
RO-nt.Txnip.C247S320 (22)
C
1/2 radius cell count
10000
8000
6000
4000
2000
0
****, +38%
Control (15)
CMV-Txnip.C247S (13)

Figure 3

Figure 4 Summary of various alleles of TXNIP in this and previous study (Xue et al., 2021). "RPE GLUT1 Removal" refers to the amount of GLUT1 immunohistochemical signal on the basal surfacxe following expression in the RPE using the Best1 promoter. "Cone Rescue: Expression in RPE" refers to cone rescue following expression only in the RPE using the Best1 promoter. "Cone Rescue: Expression in Cones" is due to expression only in cone photoreceptors using the RedO promoter.

Abbreviations: Y (x%): Yes with x% increase compared to AAV-H2BGFP control; N: No; NT: Not tested. N.Txnip, N-terminal portion of TXNIP; C.TXNIP.C247S, C-terminal portion of TXNIP.C247S mutant allele; sC.TXNIP: a shorter version of C-terminal portion of TXNIP; nt.Txnip.C247S, no tail version TXNIP.C247S mutant allele; Arrestin N-, N-terminal arrestin domain; Arrestin C-, C-terminal arrestin domain; PPxY, a motif where P is proline, x is any amino acid and Y is tyrosine.

	RPE GLUT1 Removal	Cone Rescue: Expression in RPE	Cone Rescue: Expression in Cones
wt Txnip (1-397aa)	Y (-66%)	N	Y (60%)
Txnip.S308A (1-397aa)	NT	NT	N
Txnip.C247S (1-397aa)	Y (-34%)	N	Y (97%)
Txnip.C247S.LL351&352AA (1-397aa)	N	Y (45%)	Y (43%)
N.Txnip (1-228aa)	N	N	N
C.Txnip.C247S (149-397aa)	Y (-74%)	Y (54%)	N
C.Txnip.C247S.LL351&352AA (149-397aa)	N	Y (58%)	NT
sC.Txnip (255-397aa)	Y (-28%)	N	NT
nt.Txnip.C247S (1-301aa)	NT	NT	Y (47%)
nt.Txnip.C247S (1-320aa)	N	Y (16%)	Y (63%)
	Cone Rescue		
CMV-Txnip.C247S	Y (38%)		
RedO-Txnip.C247S + Best1-Nrf2	Y (14% increase to RedO-Txnip.C247S)		

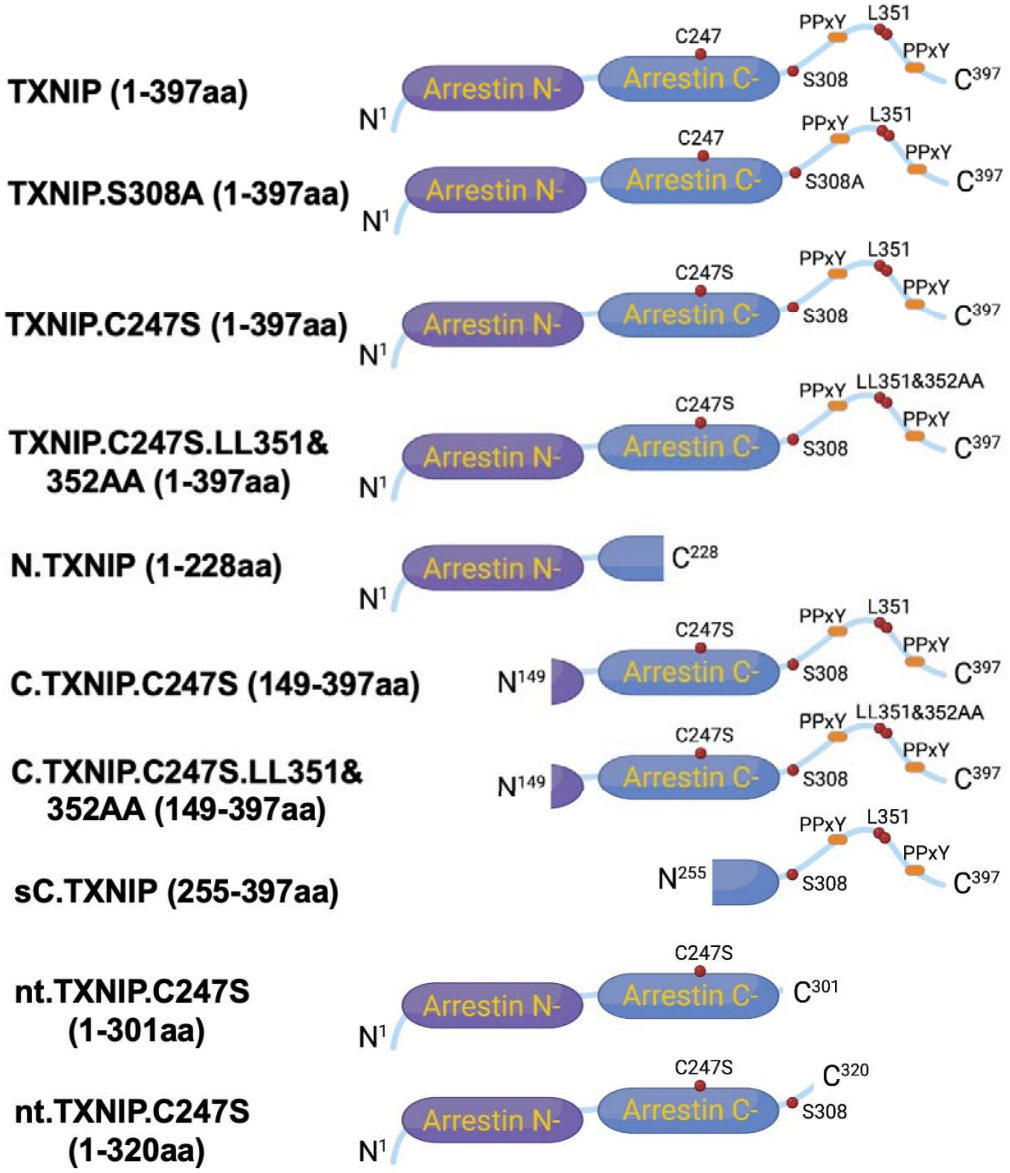

Figure 4

Figure 5 Effect of knockdown of Hsp90ab1 in RP cones *in vivo*.

A. AAV8-RO1.7-Hsp90ab1-FLAG (1×10^9 vg/eye) co-injected with shNC (non-targeting shRNA control, AAV8-RedO-shRNA, 1×10^9 vg/eye) or co-injected with Hsp90ab1 shRNAs #a, #b, #c (AAV8-RedO-shRNA, 1×10^9 vg/eye) in P20 wt retina, all also injected with AAV8-RedO-H2BGFP (2.5×10^8 vg/eye) to track the infection. Magenta: anti-FLAG; green: anti-GFP; gray: DAPI. Right panel:

B. The quantification of FLAG intensity from multiple fields of inner segment regions in A. The number in the square brackets '[]' indicates the number of images taken from regions of interest of one retina, in each condition.

C. Representative P50 *rd1* flat-mounted retinas injected with shNC, shHsp90ab1(#a), shHsp90ab1(#b), or shHsp90ab1(#c) (AAV8-RedO-shRNAs, 1×10^9 vg/eye, plus AAV8-RedO-H2BGFP, 2.5×10^8 vg/eye).

D. Quantification of H2BGFP-positive cones within the center of P50 *rd1* retinas transduced with shNC, shHsp90ab1(#a, #b, #c) (same as in C).

E. Representative P50 *rd1* flat-mounted retinas with H2BGFP (gray)-labeled cones transduced with Txnip.C247S or Txnip.C247S + shHsp90ab1 (AAV8-RedO-Txnip.C247S, 1×10^9 vg/eye; AAV8-RO1.7-shHsp90ab1(#a or #c), 1×10^9 vg/eye; plus AAV8-RedO-H2BGFP, 2.5×10^8 vg/eye).

F. Quantification of H2BGFP-positive cones within the center of P50 *rd1* retinas transduced with Txnip.C247S or Txnip.C247S + shHsp90ab1 (same as in E).

G. Representative P50 *Parp1*$^{-/-}$ *rd1* flat-mounted retinas with H2BGFP (gray)-labeled cones transduced with shNC (non-targeting shRNA control, AAV8-RedO-shRNA, 1×10^9 vg/eye; plus AAV8-RedO-H2BGFP, 2.5×10^8 vg/eye) or shHsp90ab1 (AAV8-RedO-shRNA #a or #c, 1×10^9 vg/eye; plus AAV8-RedO-H2BGFP, 2.5×10^8 vg/eye).

H. Quantification of H2BGFP-positive cones within the center of P50 *Parp1*$^{-/-}$ *rd1* retinas transduced with shNC or shHsp90ab1 (same as in G).

Error bar: standard deviation. Statistics: ANOVA and Dunnett's multiple comparison test for B and D; two-tailed unpaired Student's t-test for F and H. NS: not significant, $p>0.05$, *$p<0.05$, **$p<0.01$, ***$p<0.001$ **** p< or <<0.0001.

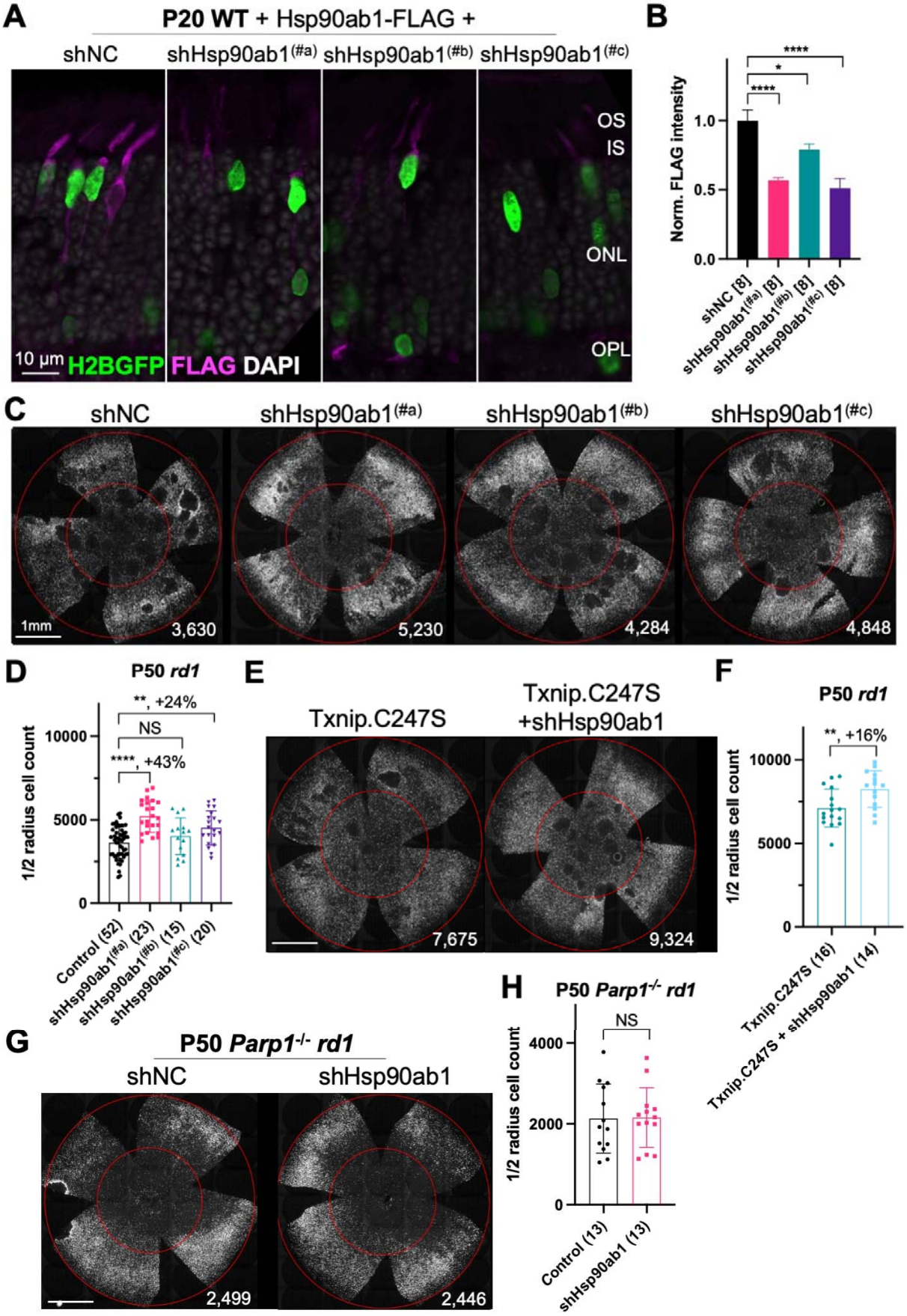
A
P20 WT + Hsp90ab1-FLAG +
shNC
shHsp90ab1(#a)
shHsp90ab1(#b)
shHsp90ab1(#c)
OS
IS
ONL
OPL
10 µm
H2BGFP
FLAG
DAPI
B
Norm. FLAG intensity
1.0
0.5
0.0
****
*
****
shNC [8]
shHsp90ab1(#a) [8]
shHsp90ab1(#b) [8]
shHsp90ab1(#c) [8]
C
shNC
shHsp90ab1(#a)
shHsp90ab1(#b)
shHsp90ab1(#c)
1mm
3,630
5,230
4,284
4,848
D
P50 rd1
1/2 radius cell count
10000
5000
0
**, +24%
NS
****, +43%
Control (52)
shHsp90ab1(#a) (23)
shHsp90ab1(#b) (15)
shHsp90ab1(#c) (20)
E
Txnip.C247S
Txnip.C247S
+shHsp90ab1
7,675
9,324
F
P50 rd1
1/2 radius cell count
10000
5000
0
**, +16%
Txnip.C247S (16)
Txnip.C247S + shHsp90ab1 (14)
G
P50 Parp1-/- rd1
shNC
shHsp90ab1
2,499
2,446
H
P50 Parp1-/- rd1
1/2 radius cell count
4000
2000
0
NS
Control (13)
shHsp90ab1 (13)

Figure 5

Figure 5-figure supplement 1 Predicted 3D protein structures of HSP90AB1 and PARP1.

A. Predicted 3D protein structures of HSP90AB1 by AI algorithm AlphaFold-2 from two angles of view.

B. Predicted 3D protein structures of PARP1 by AI algorithm AlphaFold-2 from two angles of view.

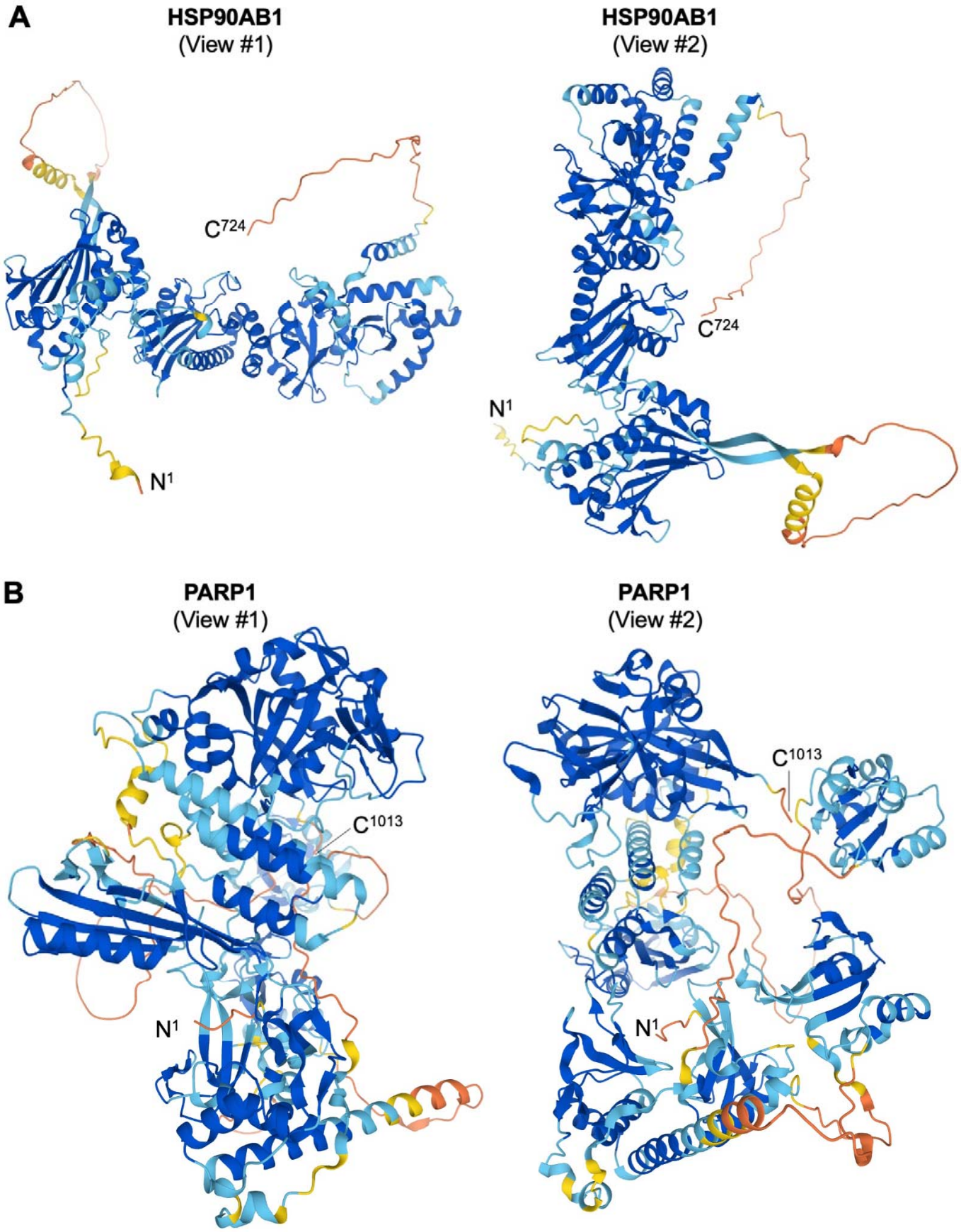

Figure 5 Supplement 1

Figure 5-figure supplement 2 Predicted 3D protein interactions among TXNIP, HSP90AB1, and PARP1 by AI algorithm AlphaFold Multimer from two angles of view. Abbreviations: Arr C-, C-terminal arrestin domain.

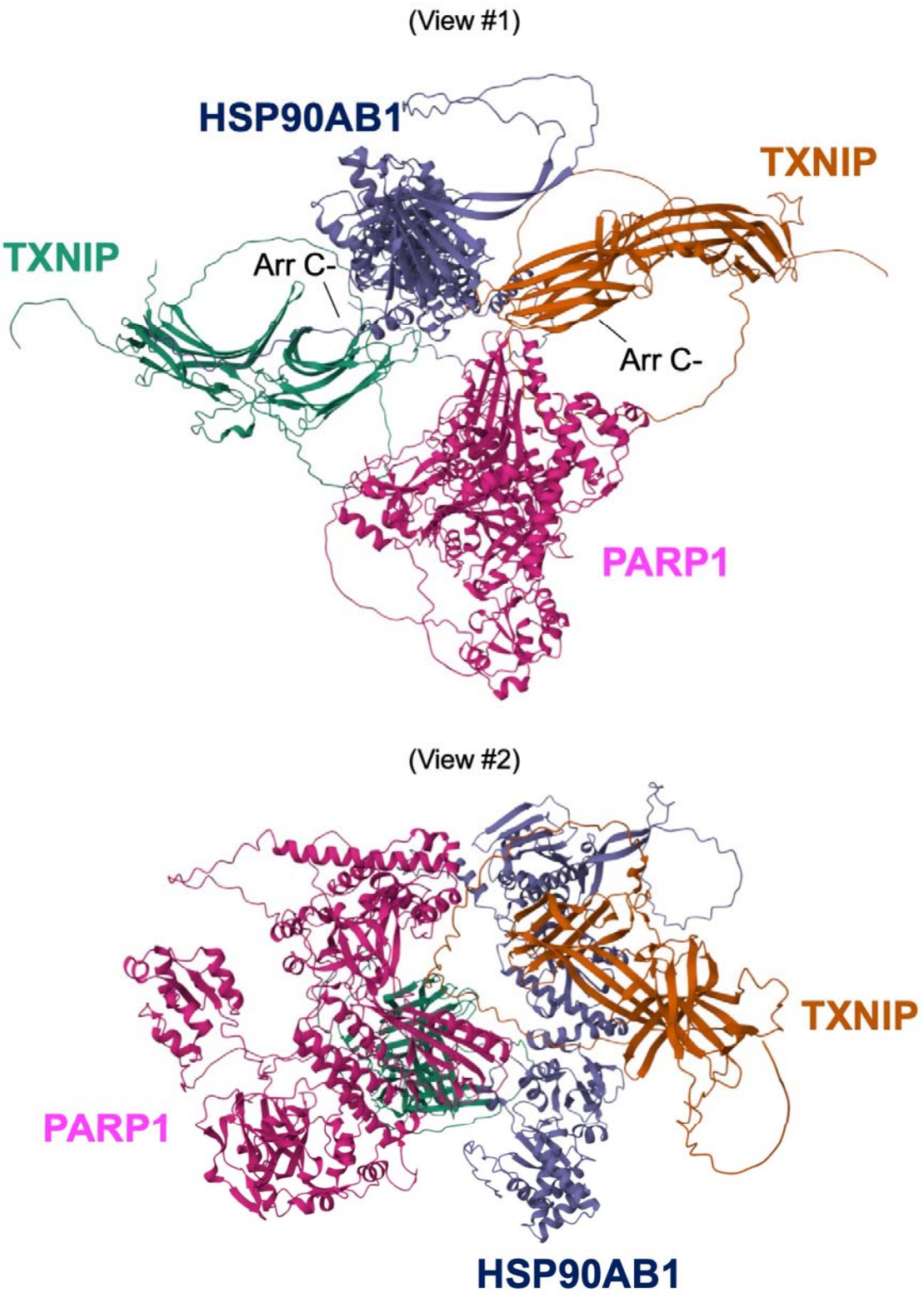

Figure 5 Supplement 2